ROYAL SOCIETY OF CHEMISTRY

PAPER

Check for updates

Beyond templates: exploring uncharted territory in anisotropic gold nanostructure-oligomer composites synthesis and electrocatalytic performance towards environmental pollutants†

Veeramani Mangala Gowri, [ID] *[ab] Theelada Panleam,[a] Jayant Giri, [ID] [cdef] Nattapong Srithongkul,[a] Krishnamoorthy Shanmugaraj,[g] Amanullah Fatehmulla[h] and Sirikanjana Thongmee*[a]

The synthesis of polymer/oligomer-stabilized metal nanostructures (MNS) opens up a wide range of possibilities, from fundamental materials science to practical applications in domains such as medicine, catalysis, sensing, and energy. Because of the versatility of this synthetic approach, it is a dynamic and ever-changing field of study. These polymers/oligomers have precise control over the nucleation and growth kinetics, allowing the production of mono-disperse MNS with well-defined properties. The protective coating provided by polymers or oligomers increased the stability and colloidal dispersity of MNS in these oligomer-MNS composites. As a result, the current research reports the electrocatalytic reduction of nitrobenzene (NB) utilizing oligomeric aminomercaptotriazole (oligo AMTa) and oligo (AMTa-AuNS) modified glassy carbon (GC) electrodes developed *via* a wet chemical technique. UV-visible spectroscopy, Fourier-transform infrared spectroscopy (FT-IR), X-ray photoelectron spectroscopy (XPS), high resolution mass spectroscopy (HR-MS), and high-resolution transmission electron microscopy (HR-TEM) approaches were used to confirm the development of oligomer and AuNS. After that, the GC electrode was directly linked to the oligo AMTa and oligo AMTa-AuNS by dipping them in the appropriate solutions. Scanning electron microscopy (SEM), electrochemical impedance spectroscopy (EIS), and cycle voltammetry (CV) were all employed to confirm the fabrication of oligo AMTa and oligo AMTa-AuNS. Eventually, the electrochemical reduction of NB occurred using the fabricated electrodes. The catalytic activity of oligo AMTa-AuNS has been observed to be more than that of the other modified electrode. As an outcome, the film was employed to determine the sensitivity level of NB, and a limit of detection (LOD) of 2.8 nM was found. The straight-forward method's practical utility was proven by measuring NB in lake sample water.

[a]Department of Physics, Faculty of Science, Kasetsart University, Bangkok, 10900, Thailand. E-mail: gowrishasha1@gmail.com; fscisjn@ku.ac.th

[b]Centre for Nanoscience and Nanotechnology, Department of Chemistry, The Gandhigram Rural Institute, Gandhigram, 624 302, Dindigul, Tamilnadu, India

[c]Department of Mechanical Engineering, Yeshwantrao Chavan College of Engineering, Nagpur, India

[d]Division of Research and Development, Lovely Professional University, Phagwara, India

[e]Centre for Research Impact & Outcome, Chitkara University Institute of Engineering and Technology, Chitkara University, Rajpura, 140401, Punjab, India

[f]Department of VLSI Microelectronics, Saveetha School of Engineering, Saveetha Institute of Medical and Technical Sciences (SIMATS), Saveetha University, Chennai 602105, TN, India

[g]Departamento de Química, Facultad de Ciencias, Universidad de Tarapacá, Avda. General Velásquez-1775, Arica, Chile

[h]Department of Physics and Astronomy, College of Science, King Saud University, Riyadh 11451, Saudi Arabia

† Electronic supplementary information (ESI) available. See DOI: https://doi.org/10.1039/d4ra07744j

1. Introduction

In light of their numerous uses in catalysis, sensing, optoelectronics, surface-enhanced Raman scattering (SERS), and other fields, as well as their unique properties (optical, electric, catalytic, biocompatible, distinct size-related electronic behavior, and good conductivity), metal nanostructures (MNS) have drawn a lot of focus recently.[1–3] Because of their mechanical strength, electrical conductivity, and corrosion stability, conducting polymer/oligomer applications have garnered considerable attention during the last three decades. They have found widespread application in optoelectronics, solar cells, light-emitting diodes, artificial muscle, super capacitors, corrosion protection, and biosensors.[3–8] Researchers are now enthusiastic about the study of polymers/oligomers incorporating MNS. The combination of conducting polymers/oligomers and MNS is predicted to improve catalytic activity.[3–8]

Chemical methods were mostly used for developing MNS-conducting polymers/oligomers composites in general.[3–8] Several studies have explored methods for synthesizing gold nanostructures (AuNS) using oligomers and polymers, including fluoroalkyl end-capped oligomers, block copolymers, and biopolymers, for enhanced stability and functionality. Techniques such as sonochemical synthesis, self-assembly, interfacial polymerization, and template-free approaches have enabled the development of diverse nanostructures, including core–shell and yolk–shell composites. There are few publications in AuNS conducting oligomers, such as Sawada *et al.*, who synthesized gold nanoparticles (AuNPs) utilizing fluoroalkyl end-capped oligomers.[9] Schubert and coworkers revealed the use of poly(ethylene oxide)-*block*-poly(α-caprolactone) copolymers to produce stable AuNPs.[10] By using a sonochemical technique, Atobe and colleagues synthesized poly(pyrrole)-AuNPs nanocomposites.[11] Self-assembly was used to produce end-capped oligomers, which were then used to synthesize fluorinated oligomeric nanocomposites.[12] Cooper and coworkers developed poly(acrylic acid) and poly(methacrylic acid) stabilized AuNPs in aqueous media in a single-step process.[13] Pradeep and coworkers described the chemical synthesis of an oligoaniline-capped gold nanostructure (AuNS) with $HAuCl_4$ as an oxidant.[4] To stabilize the AuNPs, biopolymers (α,ω-dithiol poly(*N*-isopropylacrylamide)) and poly(ethylene glycol) were utilized.[14] Kannan and John developed gold-5-amino-2-mercapto-1,3,4-thiadiazole core–shell nanoparticles and used them for the electrochemical detection of L-cysteine.[15] Taniguchi and co-workers used potassium persulfate as an initiator for producing poly[2-(*N*,*N*′-dimethyl amino)ethyl methacrylate] core–shell AuNPs.[16] Efficient interfacial polymerization was used to develop a core–shell composite with polypyrrole (PPy) covering on Au nanorods which exhibits good photostability and high two-photon photothermal efficiency.[17] Hou *et al.* described how to fine-tune the LSPR response of the GNR–PANI core–shell nanoparticles by covering the PANI nanoshells in a thickness-controlled manner.[18] In contrast to the widely employed sacrificial template approach, the recommended sacrificial template-free procedure develops PANI–Au yolk–shell nanostructures.[19] Yang *et al.* reported gold nanoparticle–graphene nanohybrids (Au–GR) and 3-amino-5-mercapto-1,2,4-triazole-functionalized multiwall carbon nanotubes (MWCNT–SH) were synthesized. A novel hybrid material, MWCNT–SH@Au–GR, was formed through the interaction between the gold nanoparticles in the two-dimensional (2D) Au–GR and the SH groups in the one-dimensional (1D) MWCNT–SH.[20] In accordance with our goal of developing reliable and effective sensing platforms, this study adopted and followed Pradeep and colleagues'[4] description of the chemical synthesis of an oligoaniline-capped AuNS using $HAuCl_4$ as an oxidant, enabling the synthesis of anisotropic AuNS specifically designed for electrocatalytic detection of environmental pollutants.

Considering that nitrobenzene (NB) is used extensively in industrial processes and that it is toxic, carcinogenic, and persistent in the environment, posing serious risks to ecosystems and human health, its measurement is essential. For the purpose of evaluating pollution, maintaining regulatory compliance, and averting hazardous exposure, NB level monitoring is crucial.[21–23] Compared to more conventional chemical and analytical procedures like spectrophotometry or chromatography,[24–26] electrochemical methods[27–32] provide a number of advantages. This method is extremely sensitive, detecting trace amounts of NB with rapid response times and low detection limits. This method is also inexpensive, require little sample preparation, and can be used with portable sensors for in-place and real-time monitoring. Furthermore, electrochemical techniques are adaptable, allowing for the simultaneous detection of multiple pollutants and the use of tailored electrode materials to enhance selectivity and sensitivity, making them an excellent choice for NB determination in a variety of environmental and industrial circumstances.[27–32]

Establishing oligomer and anisotropic oligomer-capped gold nanostructures (AuNS) with 3-amino-5-mercapto-1,2,4-triazole (AMTa) as a monomer is the purpose of this investigation. The developed oligo AMTa and oligo AMTa-AuNS were subsequently investigated on glassy carbon (GC) electrodes for their electrocatalytic performance of NB reduction. We chose AMTa as a monomer because its electropolymerized film has exceptional electrocatalytic characteristics, as revealed in our lab publication.[33] There are no reports are available for the preparation of oligomer capped AuNS using AMTa as monomer. Both reduction of metal ion and oxidation of monomer taking place simultaneously. In this preparation, AMTa can act as both reducing agent as well as capping agent. $HAuCl_4$ was act as oxidizing agent which oxidizes the monomer to oligomer. The prepared oligo AMTa-AuNS were highly stable for several months. The main advantage of the work is to prepare the anisotropic oligo AMTa-AuNS without the aid of any template or shape directing agent like polyvinylpyrrolidone (PVP) and cetyltrimethylammonium bromide (CTAB). Here, the monomer was acting as templating agent. Through Michael's nucleophilic addition reaction,[27,32,34] the oligo AMTa and oligo AMTa-AuNS were assembled on the GC electrode by simple immersion without the need for any linker. UV-visible spectroscopy and HR-TEM studies were used to characterize the development of anisotropic AuNS. The fabricated electrode was subsequently effectively utilized for NB monitoring. An assessment of the NB concentration in a lake water sample demonstrated the practical implications of the oligo AMTa-AuNS modified electrode.

2. Experimental

2.1. Materials and methods

Citric acid (CA), 3-amino-5-mercapto-1,2,4-triazole (AMTa), *N*-methyl-2-pyrrolidone (NMP), sodium dihydrogen phosphate dihydrate ($NaH_2PO_4 \cdot 2H_2O$) and disodium hydrogen phosphate dihydrate ($Na_2HPO_4 \cdot 2H_2O$) were purchased from Merck, India and were used as received. Glassy carbon (GC) plates were purchased from Alfa-Aesar. Na_2HPO_4 and $Na_2H_2PO_4$ were used to prepare phosphate buffer (PB) solution (pH 7.2). Double distilled (DD) water was used to prepare the solutions used in the present work.
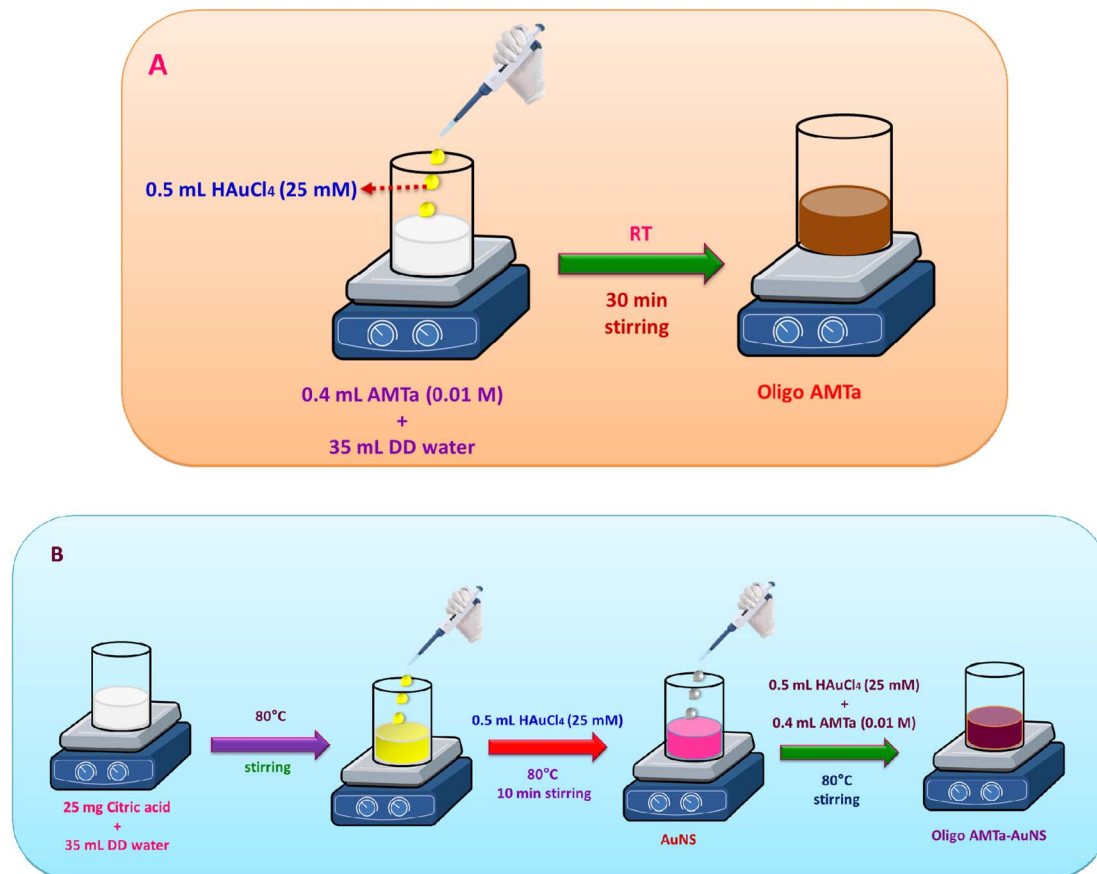
Scheme 1 Synthetic strategy of (A) oligo AMTa and (B) oligo AMTa–AuNS by wet chemical method.

Absorption spectra were measured using PerkinElmer lambda 35 and JASCO V-750 UV-visible spectrophotometer. XPS measurement were done by using PHI 5000 VERSAPROBE scanning ESCA Microscope. The FT-IR measurements were carried out in JASCO FT-IR-460 plus model. High resolution transmission electron microscopy (HR-TEM) images were taken from JEOL JEM 2100 (200 kV). High resolution-mass spectroscopy (HR-MS) were obtained on an Agilent 6530 Q-TOF-MS (Agilent Technologies, USA). Electrochemical measurements were carried out with CHI model 643B (Austin, TX, USA) Electrochemical analyzer. The measurements were performed in a conventional two-compartment three electrode cell with a polished 3 mm glassy carbon electrode (GCE) as a working electrode, a platinum wire as a counter electrode and NaCl saturated Ag/AgCl electrode as a reference electrode. All the electrochemical experiments were carried out under the nitrogen atmosphere at room temperature. Scanning electron microscope (SEM) measurements were carried at VEGA3 TESCAN, USA. For SEM and EDAX analysis GC plate was used as a substrate.

2.2. Synthesis of oligo AMTa and oligo AMTa-AuNS by chemical method

In 35 mL of DD water, 400 μL of the 0.01 M AMTa aqueous solution was dissolved to produce the oligo AMTa. The mixture was agitated for thirty minutes at ambient temperature.

Following that, the reaction mixture was mixed with 500 μL of 25 mM $HAuCl_4$. After an hour of stirring the reaction mixture, a brownish-black colored solution appeared, signifying the synthesis of oligo AMTa. After centrifuging the mixture at 4300 rpm, 5 mL of NMP solvent was used to dissolve the oligo AMTa powder, which had a brownish-black appearance. After several months at room temperature, the solution remained quite stable.

After dissolving 25 mg of citric acid in 35 mL of DD water and keeping the mixture at 80 °C, 0.5 mL of 25 mM $HAuCl_4$ was added to produce the oligo AMTa-AuNS. After ten minutes, the color transformed from yellow to pink. Following that, 400 μL of 0.01 M aqueous AMTa and 500 μL of 25 mM $HAuCl_4$ were added. The production of oligo AMTa-AuNS was demonstrated by the emergence of a colloidal bluish-pink color solution after five minutes of heating. Then, the solution was centrifuged for 4300 rpm and the obtained black color powder was dissolved in 5 mL NMP solvent. The solution was stored at room temperature and it was highly stable for several months. Scheme 1 illustrates the synthetic strategy of oligo AMTa and oligo AMTa-AuNS by wet chemical method.

2.3. Preparation of oligo AMTa and oligo AMTa-AuNS modified GC electrode

By direct immersion, the resulting oligo AMTa-AuNS and oligo AMTa were modified on the surface of GC electrode. For 12

hours, the freshly washed GC electrode was placed in the oligo AMTa and oligo AMTa-AuNS solution (Scheme S1†). GC/oligo AMTa-AuNS electrode was a label assigned to the electrode. Following Michael's nucleophilic addition of the amine group to the olefinic bond in the electrode, the amine group attaches itself to the GC electrode.[27,32,34] After that, DD water was used to wash the electrodes. Scheme S1† depicted how the oligo AMTa and oligo AMTa-AuNS were attached to the GC electrode.

3. Results and discussion

3.1. Different techniques for characterization of oligo AMTa and oligo AMTa-AuNS

The π–π^* transition of the heterocyclic triazole ring induced the absorption band of AMTa monomer in NMP solvent to be noticed at 317 nm (Fig. 1A). The resulting oligo AMTa's UV-visible spectrum in NMP solvent is displayed in Fig. 1B. It shows the sharp absorption peak at 301 nm. The absorption peak of oligo AMTa-AuNS in NMP solvent was observed at 304, 555 and 846 nm (Fig. 1C). The π–π^* transition of AMTa's heterocyclic ring was responsible for the absorbance peak detected at 304 nm. The results of the UV-visible spectrum indicate that AMTa most likely serves as a stabilizing agent as well as a reducing agent during the synthesis of AuNS. Consistent peak morphologies and absorbance, which represent

prevention of aggregation, suggest stability, whereas the distinctive surface plasmon resonance peaks of AuNPs indicate the reducing effect. Oxidation of AMTa generates the electrons which reduces the auric ions into 'Au' atoms and simultaneously.[4] The reduced auric acid was oxidized the AMTa into oligo AMTa. The absorption band that appeared at 555 nm is caused by the surface plasmon resonance (SPR) band of AuNS. The anisotropic structure of AuNS is responsible for the absorption band at approximately 846 nm. HR-TEM (Fig. 3) analysis provided more evidence for the anisotropic structure of AuNS.

Also, FT-IR spectroscopy was applied to evaluate the obtained oligo AMTa and oligo AMTa-AuNS powders. Fig. S1† demonstrates the FT-IR spectra of the formed oligo AMTa and oligo AMTa-AuNS, as well as the solid AMTa monomer. Table S1† provides an overview of the IR bands for oligo AMTa and oligo AMTa-AuNS as well as their assignments. In contrast to AMTa, the oligo AMTa and oligo AMTa-AuNS demonstrate a new peak at 1449 and 1435 cm^{-1}, respectively (curves b and c). Curve a show an insignificant stretching doublet for AMTa at 3298 and 3268 cm^{-1}. Curves b and c show that these bands do not occur for oligo AMTa and oligo AMTa-AuNS, demonstrating that –NH$_2$ groups are involved in the oligomerization process.[33,35] Therefore, oligo AMTa and oligo AMTa-AuNS exhibit a stretching band at 1449 and 1435 cm^{-1}, respectively,
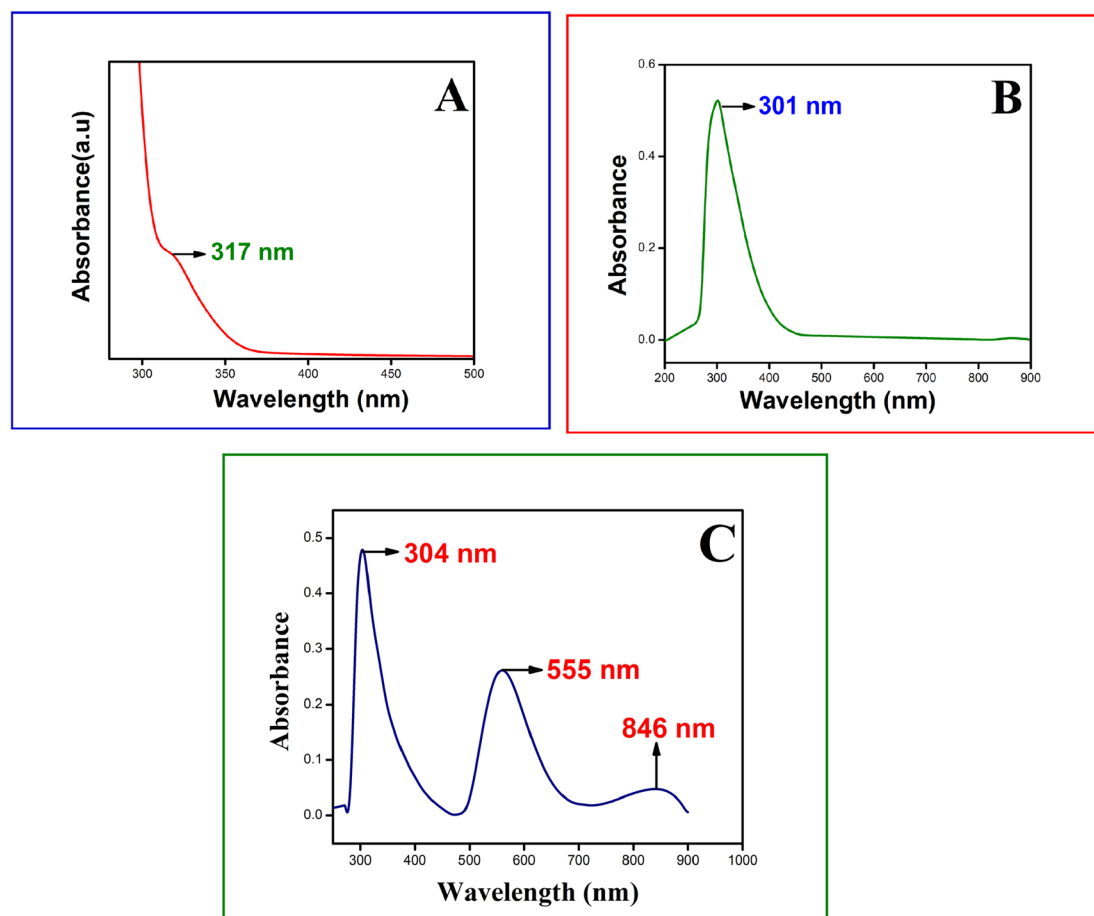

Fig. 1 UV-visible spectra of (A) AMTa, (B) oligo AMTa and (C) oligo AMTa-AuNS solutions.

corresponding to –N=N–,[33–37] demonstrating that during oligomerization, –NH$_2$ groups were converted into –N=N– groups; in contrast, oligo AMTa did not exhibit this peak. The curve a further show that the AMTa has a peak at 2615 cm^{-1}, correlating to the –SH group. This peak disappeared at oligo AMTa and oligo AMTa-AuNS, indicating that S–S[23,33] linkage is the mechanism by which oligomerization occurs (curves b and c). Beyond the peak displayed by the AMTa with greater shift, the oligo AMTa and oligo AMTa-AuNS exhibit a peak at 1678 and 1680 cm^{-1} (curves b and c), respectively.[33] The peaks at 1678 and 1680 cm^{-1} demonstrate the C=N stretching vibration. The C–N stretching vibration is apparent by the peak that both oligo AMTa and oligo AMTa-AuNS present at 1282 and 1296 cm^{-1}, respectively.[33]

The XPS spectra for oligo AMTa and oligo AMTa-AuNS are displayed in Fig. S2† and 2. The AMTa molecule and Au particles are present on the surface of oligo AMTa-AuNS, as shown by the acquired XPS spectra. Two peaks, separated by 3.7 eV, may be observed in the Au 4f spectrum at 87.6 and 83.9 eV. These peaks are consistent with Au's zero valent nature and demonstrate its 4f$_{7/2}$ and 4f$_{5/2}$, respectively[38] (Fig. 2e). The gold atom appears as Au^0 since there is no binding energy (BE) at 84.9 eV, which corresponds to Au^{3+} (Fig. 2e).[38,39] This suggests that nanostructures have successfully formed. However, 84.8 eV in the case of oligo AMTa suggests that the gold atom does not exist as Au^0 (Fig. S2d†). It verifies that no gold nanoparticle has been developed. At 163.8 and 167.9 eV, the S2p region of the oligo AMTa-AuNS deconvoluted into two component peaks, which were linked to sulfur bound to AuNS and heterocyclic sulfur, respectively[39] (Fig. 2d). The secondary amine nitrogen (–NH–) and positively charged nitrogen (–N$^+$H–) of the oligo AMTa-AuNS were responsible for the two component peaks that were deconvoluted into the XPS for N 1s spectra (Fig. 2b).[39] These peaks were located at 399.9 and 403.3 eV, respectively. The secondary amine nitrogen (–NH–) and imine nitrogen (=NH) are responsible for the two

component peaks at 399.9 and 396.7 eV in the oligo AMTa N 1s spectra, respectively[39] (Fig. S2b†). The O 1s spectrum of oligo AMTa-AuNS revealed two major peaks at 531.2 and 533.2 eV, and these are associated with hydroxyl (C–O) and carbonyl (C=O), respectively (Fig. 2c). Two component peaks at 285.0 and 287.0 eV, which were linked to C–N and C=N, respectively,[39] were identified using deconvolution of the oligo AMTa C 1s spectra (Fig. S2a†). The C 1s spectra for oligo AMTa-AuNS were fitted into two peaks at 285.3 and 287.3 eV (Fig. 2a). At 285.3 eV, C–N was demonstrated to be the predominant BE. The C=N is represented by the tiny peak at 287.3 eV (Fig. 2a). The chemical oligomerization in both scenarios proceeds via –NH and N=N, as evidenced by the lack of BE at 284.0 eV for C–C or C=C.[39]

HR-TEM was utilized to analyze the morphology of the oligo AMTa and oligo AMTa-AuNS. The resulting oligo AMTa and oligo AMTa-AuNS powders have been dissolved in NMP solvent, drop cast onto copper grid, and then dried for HR-TEM examination. The HR-TEM images of oligo AMTa and oligo AMTa-AuNS at several magnifications are displayed in Fig. 3. The HR-TEM images exhibit the cloud-like structure of oligo AMTa (Fig. 3a–c). The oligomeric network was also seen in the back ground of the TEM image. The HR-TEM image reveals that AuNS are in pyramid, boat, rod, triangular, pentagonal and hexagonal shapes (Fig. 3d–f). Fig. S3† shows the SAED pattern of the oligo AMTa and oligo AMTa-AuNS. The SAED pattern oligo AMTa indicates the crystalline nature of the oligo AMTa (Fig. S3a†). Fig. S3b† displays the crystallinity nature of oligo AMTa-AuNS as demonstrated by its SAED pattern. The crystallinity nature increases from oligo AMTa to oligo AMTa-AuNS was also seen in the SAED pattern. This is due to the existence of metal nanostructure on the surface of the oligo AMTa which increase the crystalline nature of the oligomer.

To achieve optimized and controlled growth of anisotropic AuNS, the study varied the concentration of the monomer AMTa and the reaction temperature. Initially, AMTa concentrations of
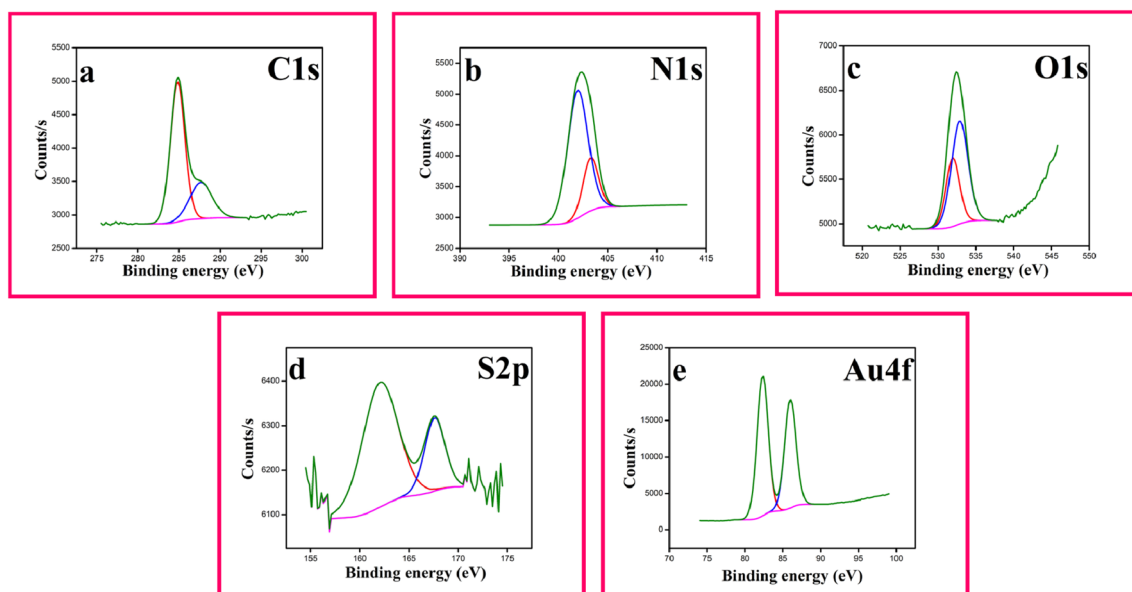

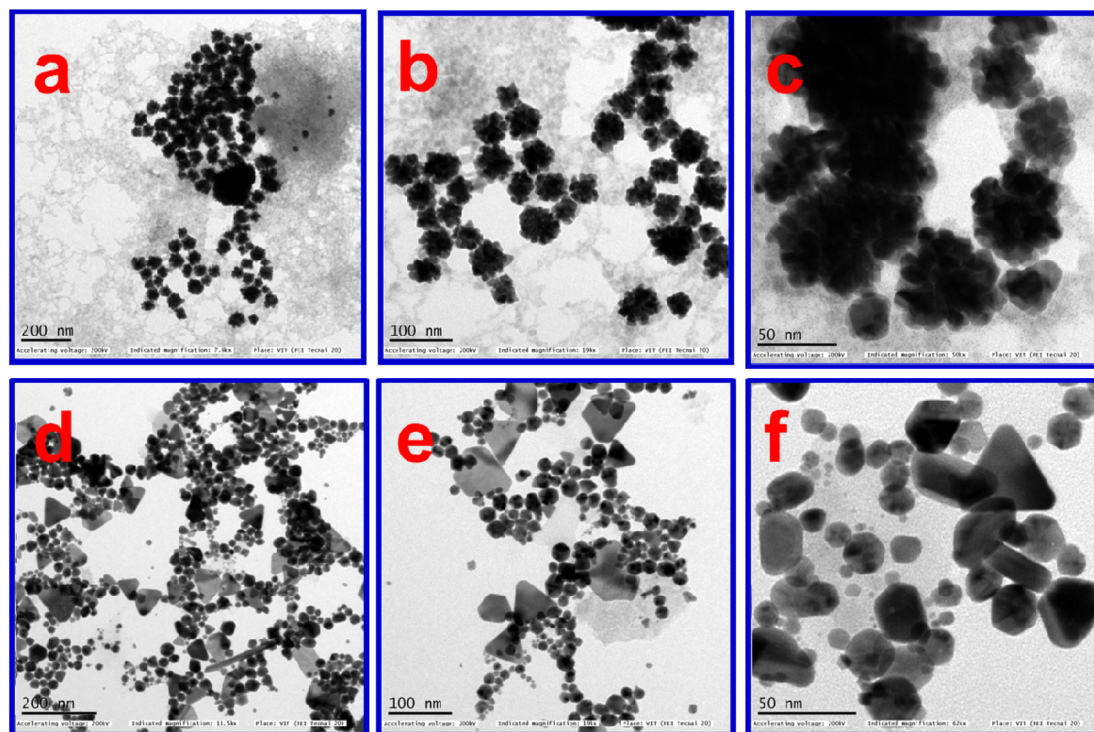Fig. 2 XPS spectra of powder oligo AMTa-AuNS: (a) C 1s, (b) N 1s, (c) O 1s, (d) S 2p and (e) Au 4f regions.

Fig. 3 TEM images of oligo AMTa (a–c) and oligo AMTa-AuNS (d–f).

500 μL, 1 mL, and 2 mL were tested at a constant synthesis temperature of 80 °C. HR-TEM images showed that using 500 μL of AMTa at 80 °C produced AuNS with distinct and controlled shapes, such as pyramidal, triangular, rod, spherical, boat, and hexagonal forms (Fig. 4a–i). This concentration appeared to support balanced and directed growth along certain crystallographic axes, likely due to an optimal interaction between AMTa and the gold surface that favours anisotropic shapes. However, at higher AMTa concentrations (1 mL and 2 mL), the images (Fig. 5a–d) revealed irregular and uncontrolled growth, producing undefined structures. The higher concentrations may lead to excessive nucleation and random deposition, resulting in uneven shapes due to the saturation of binding sites on the nanostructures' surface, which disrupts controlled anisotropic growth.

The study also explored the effects of reaction temperature by adjusting it to 60 °C, 80 °C, and 100 °C while keeping the AMTa concentration constant at 500 μL. The optimized temperature of 80 °C yielded controlled anisotropic shapes, but deviations from this temperature produced uneven, irregular structures (Fig. 5e–h). At 60 °C, lower reaction kinetics may hinder directed growth, causing incomplete and less defined structures, while at 100 °C, faster reaction rates likely lead to rapid, random growth, also resulting in poorly defined shapes. Additionally, a control experiment synthesizing pure gold nanoparticles (AuNPs) without AMTa confirmed that, in the absence of AMTa, gold naturally forms spherical particles, as shown in Fig. 5i and j. This result highlights the critical role of AMTa in promoting anisotropic growth by selectively binding to certain facets of gold, particularly under the optimized

conditions of 500 μL AMTa at 80 °C. Thus, the results emphasize that both monomer concentration and reaction temperature significantly influence the controlled growth of anisotropic AuNS, with the optimal conditions being crucial to achieving the desired shapes and stability.[4,9–20] The controlled growth of anisotropic AuNS is achieved by optimizing the monomer (AMTa) concentration and reaction temperature. At 500 μL AMTa and 80 °C, HR-TEM reveals well-defined pyramidal, triangular, and hexagonal shapes due to balanced interactions guiding anisotropic growth. Higher AMTa concentrations or non-optimal temperatures disrupt this control, leading to irregular structures, while the absence of AMTa results in spherical particles, emphasizing its critical role.

Furthermore, HR-MS was employed to investigate the resulting oligo AMTa and oligo AMTa-AuNS. The HR-MS of oligo AMTa and oligo AMTa-AuNS is displayed in Fig. 6. The measured m/z peaks range from 285 to 1420, which are indicative of distinct molecular ion species. molecular mass of AMTa monomer ($m/z = 116$) was absent in the HR-MS spectrum suggesting that AMTa may be converted to oligomer or polymer. Fig. 6a shows the HR-MS of oligo AMTa. The peak at $m/z = 564.08$ corresponds to the molecular ion of five monomers attached in a chain indicating the formation of oligomeric AMTa. In addition, the presence of tetrameric form of AMTa was confirmed from the m/z peak at 435.03. The presence of m/z peaks at 685.43 and 784.49 were corresponds to molecular ion of four and five monomers attached with metallic gold respectively. Fig. 6b shows the HR-MS of oligo AMTa-AuNS. The peaks observed at 581.18 and 857.23 were corresponds to molecular ion of pentameric form and heptameric form of AMTa
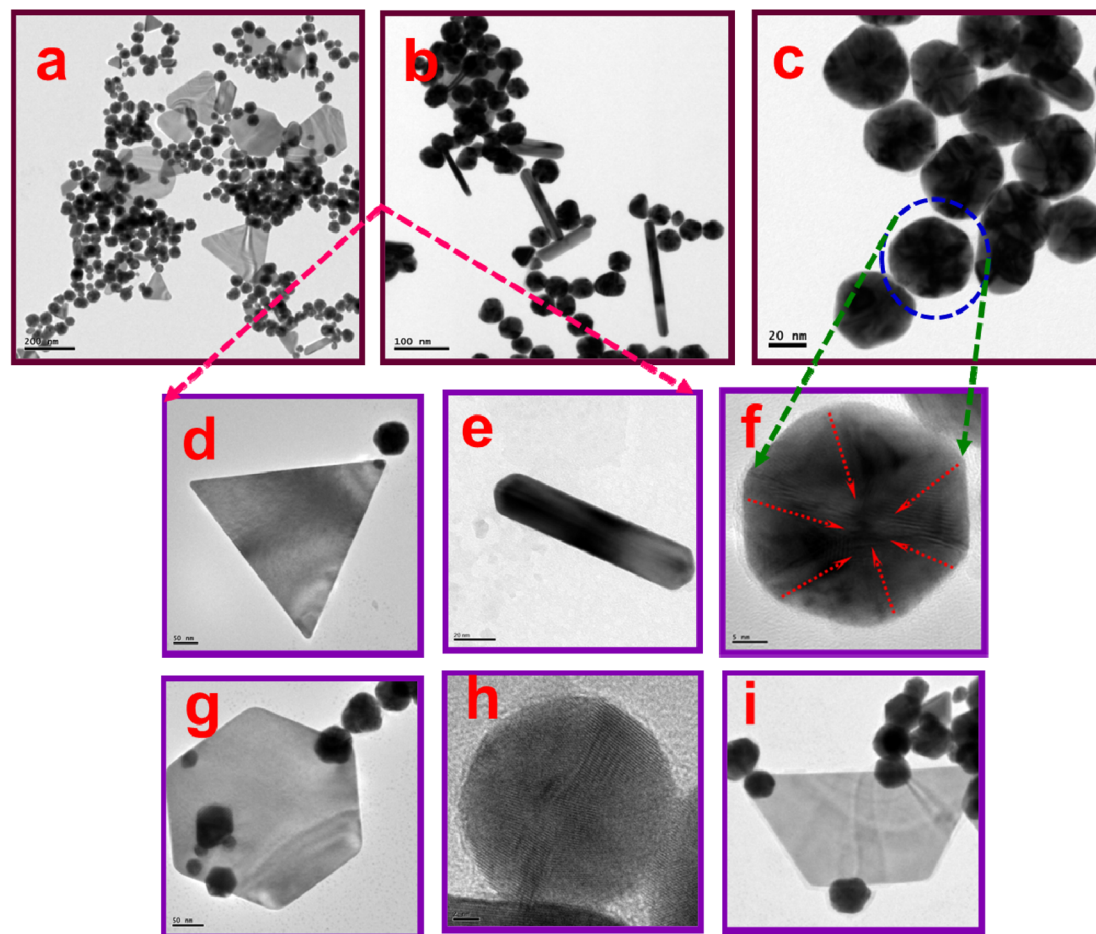
Fig. 4 HR-TEM images for (a–c) controlled shapes of anisotropic oligo AMTa-AuNS synthesized by 500 μL AMTa addition at 80 °C reaction temperature and (d–i) HR-TEM images of magnified view of (d) triangle, (e) rod, (f) pyramid, (g) hexagonal (h) spherical and (i) boat shaped anisotropic oligo AMTa-AuNS.

respectively. In addition, the presence of *m/z* peaks appeared at 784.49 which confirmed five monomers was attached with metallic gold respectively. The HR-MS spectra clearly showed that polymeric AMTa was not formed. Scheme S2† shows the schematic representation of oligo AMTa-AuNS.

The role of oligo AMTa in the synthesis of AuNS is crucial for understanding their formation and subsequent applications, particularly in electrocatalysis. AMTa serves not only as a stabilizing agent but also as a shape-directing agent that influences the morphology of AuNPs. The unique chemical structure of AMTa, which includes thiol groups, allows it to interact strongly with gold surfaces.[15,20] This interaction enables selective adsorption on specific crystallographic facets of the growing nanoparticles, leading to anisotropic growth patterns.[15,20] The mechanism by which AMTa promotes anisotropic growth can be attributed to its ability to cap certain facets while allowing others to grow unimpeded. The selective adsorption of AMTa modifies the growth dynamics of gold atoms during nucleation and subsequent growth phases. As gold is deposited, the presence of AMTa creates a kinetic barrier that hinders the addition of gold atoms to the capped facets, allowing for a greater deposition rate on unprotected facets. This differential growth rate results in a non-uniform particle shape, with specific orientations and geometries that are characteristic of anisotropic nanoparticles.[15,20]

3.2. Analysis of GC substrates modified with oligo AMTa and oligo AMTa-AuNS using SEM

SEM was used to further evaluate the modified GC plate containing oligo AMTa and oligo AMTa-AuNS. The resulting oligo AMTa and oligo AMTa-AuNS powders were dissolved in NMP solvent for the SEM analysis, and the GC plate was cleaned and immersed in each solution for 12 hours. The SEM pictures of the coated oligo AMTa and oligo AMTa-AuNS on GC plates are displayed in Fig. S4.† The SEM picture of the GC plate coated with oligo AMTa reveals spherical particles covering the entire region (Fig. S4a†). It was discovered that the particles were 2.6 μm in size. The morphology altered from an anisotropic to an aggregate-like shape after the oligo AMTa-AuNS was attached to the GC substrate (Fig. S4b†).

3.3. Electrochemical characterization of oligo AMTa-AuNS on GC electrode surface

The CVs obtained in 0.2 M PBS (pH 7.2) for the GC/oligo AMTa-AuNS electrode is displayed in Fig. S5.† The reduction peak
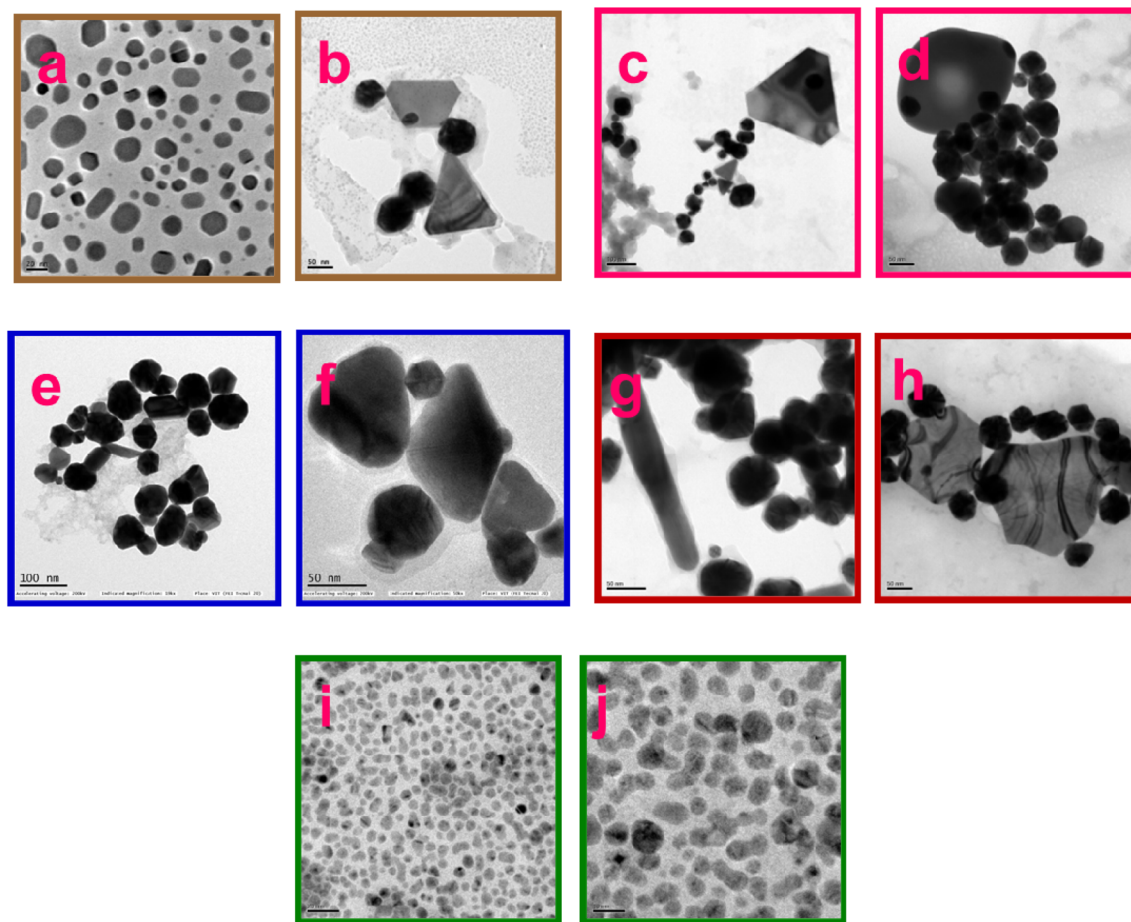
Fig. 5 HR-TEM images uncontrolled growth of anisotropic oligo AMTa-AuNS synthesized by (a and b) 1 mL AMTa at 80 °C, (c and d) 2 mL AMTa at 80 °C, (e and f) 500 μL AMTa at 60 °C, (g and h) 500 μL AMTa at 100 °C and (i and j) pure AuNPs.

appears at 0.42 V and the oxidation peak appears at 0.98 V on the GC/oligo AMTa-AuNS electrode.[40,41] In the PB solution, the attachment of gold oxide develops redox peaks. To access the electronic relationship between the GC/oligo AMTa, GC/oligo AMTa-AuNS, and unmodified GC electrodes, a further $[\text{Fe(CN)}_6]^{3-/4-}$ redox probe was employed. The CVs recorded in 0.2 M PB solution (pH 7.2) containing 1 mM $\text{K}_3[\text{Fe(CN)}_6]/\text{K}_4[\text{Fe(CN)}_6]$ for unmodified GC, GC/oligo AMTa, and GC/oligo AMTa-AuNS electrodes are displayed in Fig. S6.† The unmodified GC electrode demonstrates a peak separation of $[\text{Fe(CN)}_6]^{3-/4-}$ of 70 mV (curve a). With an increase in peak current, the GC/oligo AMTa electrode demonstrates a peak separation of 140 mV for $[\text{Fe(CN)}_6]^{3-/4-}$ (curve b). Nevertheless, $[\text{Fe(CN)}_6]^{3-/4-}$ (curve c), the GC/oligo AMTa-AuNS electrode improved both the peak current and peak separation, by 185 mV. This indicates that the oligo AMTa and oligo AMTa-AuNS enhanced the redox probe's electron transport. This result confirmed by the successful attachment of the oligo AMTa and oligo AMTa-AuNS on GC electrode surface.

The electroactive surface area (EAS) for the unmodified GC, GC/oligo AMTa, and GC/oligo AMTa-AuNS electrodes were determined using the Anson equation.[42,43] The EAS for unmodified GC, GC/oligo AMTa and GC/oligo AMTa-AuNS

electrodes were appeared at 0.06, 0.23, and 0.55 cm^2, respectively. The discrepancy in EAS was ascribed to the varied shape of oligo AMTa-AuNS composites resulting from the direct immersion. The surface area of the oligo AMTa-AuNS modified electrode was 9.2 and 2.4 times greater than unmodified GC and GC/oligo AMTa electrodes, respectively. Among the various modified electrodes, oligo AMTa-AuNS modified electrode outperforms than other electrodes in terms of EAS.

3.4. Characterization of oligo AMTa-AuNS modified GC electrode by EIS

Further, electrochemical impedance spectroscopy (EIS) was used to characterize the resulting GC/oligo AMTa, GC/oligo AMTa-AuNS electrodes. The Nyquist plots for unmodified GC, GC/oligo AMTa and GC/oligo AMTa-AuNS electrodes in 0.2 M PB solution (pH 7.2) containing 1 mM $\text{K}_3/\text{K}_4[\text{Fe(CN)}_6]$ are shown in Fig. 7. The charge transfer resistance (R_{CT}) values of 18, 10 and 4 kΩ were found for unmodified GC, GC/oligo AMTa and GC/oligo AMTa-AuNS electrodes, respectively. Using the previously reported equation,[43,44] the electron transfer rate constant (k_{et}) value for unmodified GC was 2.09, 3.65 for GC/oligo AMTa and 8.36×10^{-4} cm^2 for GC/oligo AMTa-AuNS electrode. The acquired k_{et} values demonstrated that the electron transfer
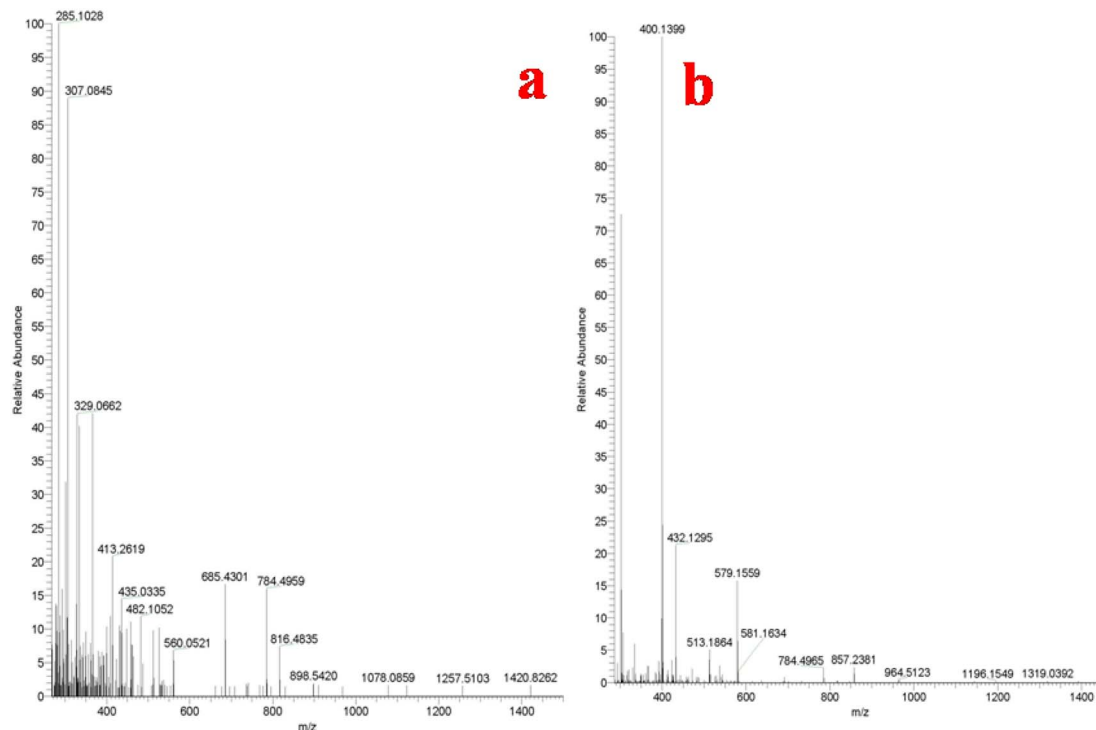
Fig. 6 HR-MS of (a) oligo AMTa and (b) oligo AMTa-AuNS.

reaction of composite modified electrode was easier than that of other modified electrodes.

3.5. NB reduction using GC/oligo AMTa-AuNS electrode

Utilizing unmodified GC, GC/oligo AMTa, GC/AuNPs and GC/oligo AMTa-AuNS composite electrodes in 0.2 M PBS (pH 7.2) (Fig. 8), 0.5 mM NB was reduced. For the unmodified GC electrode, the reduction peak was found at −0.70 V in the scrutinized potential range (curve b). The electrocatalytic activity of gold nanoparticles (AuNPs) without an oligomer was also
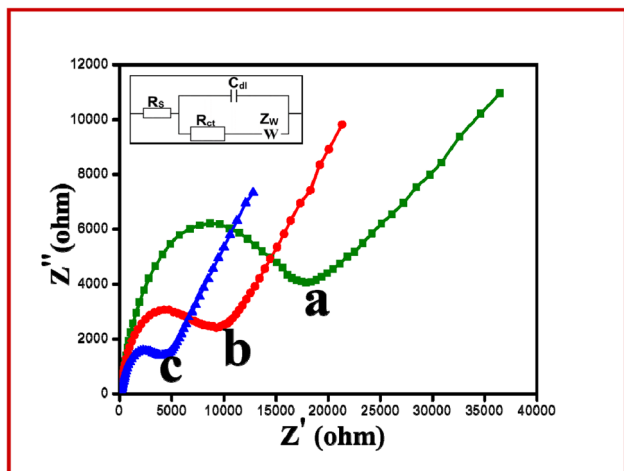

Fig. 7 A Nyquist plot for (a) unmodified GC, (b) GC/oligo AMTa, and (c) GC/oligo AMTa-AuNS electrodes in 1 mM $K_3[Fe(CN)_6]/K_4[Fe(CN)_6]$ containing 0.2 M PB solution (pH 7.2) at scanning frequencies from 0.01 to 100 000 Hz.

investigated for the comparison study. In contrast, the GC/oligo AMTa, GC/AuNPs and GC/oligo AMTa-AuNS electrodes demonstrate a substantial reduction in the peak at −0.62, −0.63 and −0.65 V, respectively, when 0.5 mM NB is present (curves c–e). Curve a demonstrates that there is no peak in the scrutinized potential range, indicating the absence of 0.5 mM NB at the GC/oligo AMTa-AuNS electrode. There is a 30 mV reduction potential shift was observed between GC/oligo AMTa and GC/oligo AMTa-AuNS electrode, which indicates the reduction reaction is more facile in GC/oligo AMTa electrode. The unmodified GC, GC/oligo AMTa, GC/AuNPs and GC/oligo AMTa-AuNS electrodes exhibit a reduction current for NB at −11, −40, −58 and −84 μA, respectively. The reduction current for the NB in the oligo AMTa-AuNS modified electrode was 7.6, 2.1 and 1.4-fold greater than unmodified GC, GC/oligo AMTa and GC/AuNPs electrodes, respectively. Its larger EAS value may have contributed to the GC/oligo AMTa-AuNS electrode's greater reduction current than the other modified electrodes.

The electrocatalytic properties of AuNS are markedly enhanced due to their unique morphology, which increases the effective surface area and exposes a greater number of active sites for catalytic reactions.[4,9–20] AuNS often exhibit improved catalytic activity compared to their isotropic counterparts, owing to the high-index facets present in these structures, which can provide more favorable adsorption sites for reactants.[4,9–20] This enhanced surface reactivity can significantly improve the kinetics of electrochemical reactions, such as the reduction of NB.[32] Furthermore, the anisotropic shapes can facilitate charge transfer processes, leading to faster electron transfer rates during reactions.[32]
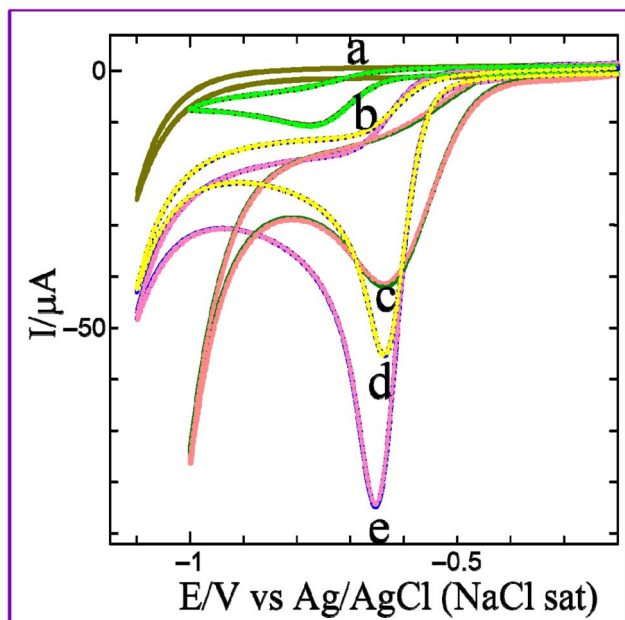
Fig. 8 CVs obtained for (a) GC/oligo AMTa-AuNS electrode in the absence of NB and (b) unmodified GC, (c) GC/oligo AMTa, (d) GC/AuNPs and (e) GC/oligo AMTa-AuNS electrodes (solid line: first cycle and dotted line: after five cycle) in the presence of 0.5 mM NB containing 0.2 M PB solution (pH 7.2) at a scan rate of 50 mV s^{-1}.

Fig. 9 DPVs obtained for each increment (curves b–o) of 100 nM NB at GC/oligo AMTa-AuNS electrode in 0.2 M PB solution (pH 7.2). (a) GC/oligo AMTa-AuNS electrode in the absence of NB. (Inset): Plot of current vs. concentration of NB.

NB reduction was accomplished by a diffusion-controlled method. This is supported by the accomplished linear plot of current vs. square root of NB concentration (Fig. S7†). Furthermore, a more substantial increase in the current of NB was reported in pH 7 when the pH was adjusted from 3 to 11. Consequently, NB was determined at a pH of 7.2, which is quite near to 7.0 (Fig. S8†).

3.6. Sensitive and selective determination of NB

NB was detected by differential pulse voltammetry (DPV) in a sensitive and selective manner. In 0.2 M PBS pH 7.2, Fig. 9 displays the DPVs of the stepwise addition of NB at the GC/oligo AMTa-AuNS electrode. When 100 nM NB was administered, a NB peak was seen at −0.60 V (curve b). Progressively the concentration of NB raised from 200 to 1400 nM (curves c–o), and the reduction current raised further while the reduction potential remained constant (a linear plot of NB reduction current versus concentration was obtained with $R^2 = 0.9978$) (Fig. 9: inset). Furthermore, the GC/oligo AMTa-AuNS electrode was employed to introduce NB in concentrations ranging from 50 nM to 1 mM for wide-range detection (Fig. S9†). The NB current increases steadily as concentration increases ($R^2 = 0.9983$; Fig. S9:† inset), with a limit of detection (LOD) of 2.8 nM (S/N = 3). The current modified electrode's performance was compared to that of previously published polymer and metal nanomaterials and composite modified electrodes (Table S2†). The sensitivity of the GC/oligo AMTa-AuNS electrode proved to be greater than that of sensors based on other polymer and metal nanoparticles materials.[41,45–53]
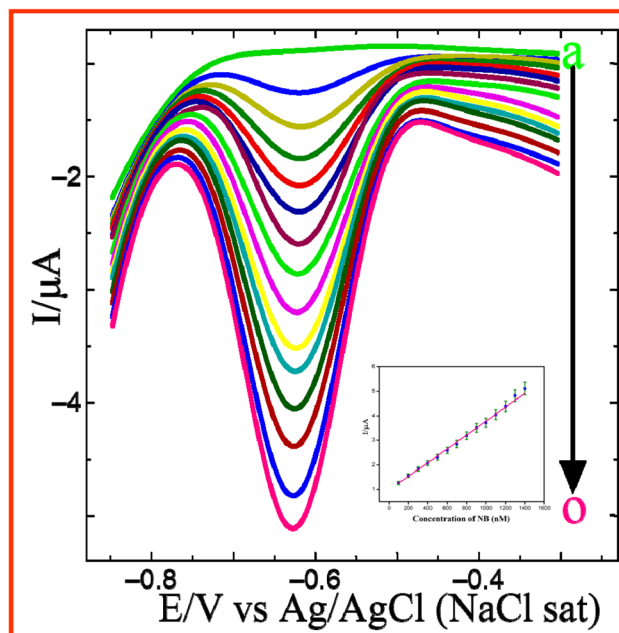
Furthermore, the selective detection of 5 µM NB containing the primary interferences was examined at the GC/oligo AMTa-AuNS electrode (Fig. S10†). When 100 µM aniline, benzene and different phenolic compounds are administered, the electrochemical response of NB remains unaltered. The electrochemical activity of NB was unaltered when 700 µM sodium, copper, chloride and nitrate ions were introduced into the same solution. These findings suggest that the GC/oligo AMTa-AuNS electrode is suitable to monitor NB in a sensitive and selective manner.

3.7. Stability and practical application

The GC/oligo AMTa-AuNS electrode's practical applicability was proved by measuring NB in lake water (Fig. S11†). Before starting the experiment, the lake water was diluted 14 times with 0.2 M PBS (pH 7.2). The GC/oligo AMTa-AuNS electrode showed no electrochemical signal for lake water (curve a). However, adding 100 nM NB to the real sample solution, on the other hand, results in a peak potential at −0.63 V (curve b). Table S3,† demonstrates that raising the amount of NB in lake water improved the reduction current, leading to a successful recovery.

Moreover, the GC/oligo AMTa-AuNS electrode's durability was evaluated by measuring the DPV of 100 nM NB at 20 minutes intervals. The NB peak at −0.63 V retains identical after eight consecutive measurements, with a relative standard deviation (RSD) of 1.3% (0.07%), demonstrating that the fabricated electrode is stable. All of these results confirm the GC/oligo AMTa-AuNS electrode's long-term storage stability. Furthermore, the reduction current was measured using five

different GC/oligo AMTa-AuNS electrodes. The modified electrode has an RSD of 1.4% (0.05%), indicating that it is exceptionally long-lasting and repeatable.

4. Conclusions

This study demonstrated an affordable and easily reproducible method for template free preparation of oligomer capped AuNS and preparing a GC electrode with oligoAMTa-AuNS for sensitive NB detection. The oligo AMTa and oligo AMTa-AuNS were synthesized chemically and studied using UV-visible spectroscopy, FT-IR, HR-MS, and XPS. Images obtained by HR-TEM depict the evolution of anisotropic oligo AMTa-AuNS structures. The oligo AMTa-AuNS was then coated on a GC surface and evaluated using SEM CV, and EIS investigations. The fabricated electrode was later employed to efficiently measure NB in neutral medium. Furthermore, in contrast to the unmodified and GC/oligo AMTa electrodes, the GC/oligo AMTa-AuNS electrode demonstrated a greater reduction current of NB. The film was employed to determine the sensitivity level of NB, and the LOD of 2.8 nM (S/N = 3) was found. A sample of lake water was successfully tested for an NB analysis using the fabricated electrode that is presently in use.

Data availability

The authors confirm that the data supporting the findings of this study are available within the article.

Conflicts of interest

There are no conflicts to declare.

Acknowledgements

References

1 J. M. George, A. Antony and B. Mathew, Metal oxide nanoparticles in electrochemical sensing and biosensing: a review, *Microchim. Acta*, 2018, **185**, 358.

2 A. Amirjani and E. Rahbarimehr, Recent advances in functionalization of plasmonic nanostructures for optical sensing, *Microchim. Acta*, 2021, **188**, 57.

3 A. John, L. Benny, A. R. Cherian, S. Y. Narahari, A. Varghese and G. Hegde, Electrochemical sensors using conducting polymer/noble metal nanoparticle nanocomposites for the detection of various analytes: a review, *J. Nanostruct. Chem.*, 2021, **11**, 1.

4 P. R. Sajanlal, T. S. Sreeprasad, A. S. Nair and T. Pradeep, Wires, plates, flowers, needles, and core–shells: diverse nanostructures of gold using polyaniline templates, *Langmuir*, 2008, **24**, 4607.

5 H. D. Kyomuhimbo and U. Feleni, Catalytic and energy storage applications of metal/polyaniline nanocomposites: a critical review, *J. Electron. Mater.*, 2022, **51**, 5568.

6 E. M. Halim, S. Chemchoub, A. E. Attar, F. E. Salih, L. Oularbi and M. E. Rhazi, Recent advances in anode metallic catalysts supported on conducting polymer-based materials for direct alcohol fuel cells, *Front. Energy Res.*, 2022, **10**, DOI: **10.3389/fenrg.2022.843736**.

7 J. Shan and Z. Ma, A review on amperometric immunoassays for tumor markers based on the use of hybrid materials consisting of conducting polymers and noble metal nanomaterials, *Microchim. Acta*, 2017, **184**, 969.

8 H. J. Kim, J. S. Lee, J. M. Park, S. Lee, S. J. Hong, J. S. Park and K. H. Park, Fabrication of nanocomposites complexed with gold nanoparticles on polyaniline and application to their nerve regeneration, *ACS Appl. Mater. Interfaces*, 2020, **12**, 30750.

9 H. Sawada, A. Sasaki, K. Sasazawa, T. Kawase, K. Ueno and K. Hamazaki, Dispersion of gold nanoparticles above the poly(methyl methacrylate) surface by the use of fluoroalkyl end-capped oligomeric aggregates, *Colloid Polym. Sci.*, 2005, **283**, 583.

10 M. Filali, M. A. R. Meier, U. S. Schubert and J. F. Gohy, Star-block copolymers as templates for the preparation of stable gold nanoparticles, *Langmuir*, 2005, **21**, 7995.

11 Z. Qi and P. G. Pickup, High performance conducting polymer supported oxygen reduction catalysts, *Chem. Commun.*, 1998, 2299.

12 H. Sawada, Synthesis of self-assembled fluoroalkyl end-capped oligomeric aggregates—Applications of these aggregates to fluorinated oligomeric nanocomposites, *Prog. Polym. Sci.*, 2007, **32**, 509.

13 Z. Wang, B. Tan, I. Hussain, N. Schaeffer, M. F. Wyatt, M. Brust and A. I. Cooper, Design of polymeric stabilizers for size-controlled synthesis of monodisperse gold nanoparticles in water, *Langmuir*, 2007, **23**, 885.

14 S. Besner, A. V. Kabashin, F. M. Winnik and M. Meunier, Synthesis of size-tunable polymer-protected gold nanoparticles by femtosecond laser-based ablation and seed growth, *J. Phys. Chem. C*, 2009, **113**, 9526.

15 P. Kannan and S. A. John, Ultrasensitive detection of l-cysteine using gold–5-amino-2-mercapto-1,3,4-thiadiazole core–shell nanoparticles film modified electrode, *Biosens. Bioelectron.*, 2011, **30**, 276.

16 T. Taniguchi, T. Inada, T. Kashiwakura, F. Murakami, M. Kohri and T. Nakahira, Preparation of polymer core–shell particles supporting gold nanoparticles, *Colloids Surf.*, 2011, **377**, 63.

17 C. Du, A. Wang, J. Fei, J. Zhao and J. Li, Polypyrrole-stabilized gold nanorods with enhanced photothermal effect towards two-photon photothermal therapy, *J. Mater. Chem. B*, 2015, **3**, 4539.

18 H. Hou, L. Chen, H. He, L. Chen, Z. Zhao and Y. Jin, Fine-tuning the LSPR response of gold nanorod–polyaniline core–shell nanoparticles with high photothermal efficiency for cancer cell ablation, *J. Mater. Chem. B*, 2015, **3**, 5189.

19 B. Zhang, T. Cai, S. Li, X. Zhang, Y. Chen, K. G. Neoh, E. T. Kang and C. Wang, Yolk-shell nanorattles encapsulating a movable Au nanocore in electroactive polyaniline shells for flexible memory device, *J. Mater. Chem. C*, 2014, **2**, 5189.

20 C. Yang, Y. Chai, R. Yuan, W. Xu and S. Chen, Gold nanoparticle–graphene nanohybrid bridged 3-amino-5-mercapto-1,2,4-triazole-functionalized multiwall carbon nanotubes for the simultaneous determination of hydroquinone, catechol, resorcinol and nitrite, *Anal. Methods*, 2013, **5**, 666.

21 S.-X. Liang, H.-K. Zhang and D. Lu, Determination of nitrobenzene in wastewater using a hanging mercury drop electrode, *Environ. Monit. Assess.*, 2007, **129**, 331.

22 R. Emmanuel, C. Karuppiah, S.-M. Chen, S. Palanisamy, S. Padmavathy and P. Prakash, Green synthesis of gold nanoparticles for trace level detection of a hazardous pollutant (nitrobenzene) causing methemoglobinaemia, *J. Hazard. Mater.*, 2014, **279**, 117.

23 A. Agrawal and P. G. Tratnyek, Reduction of nitro aromatic compounds by zero-valent iron metal, *Environ. Sci. Technol.*, 1995, **30**, 153.

24 X. Yang, W. Liu, Y. Ren, X. Hou and J. Li, Highly sensitive fluorescent sensing for nitrobenzene of CD[II] complexes based on three isomers and a bis-imidazole ligand, *Molecules*, 2024, **29**, 2475.

25 X. Zhao, C. Li, H. Zeng, X. Gu and J. Zheng, Determination of nitrobenzene potential genotoxic impurities in nifedipine with GC-MS, *J. Pharm. Biomed. Anal.*, 2024, **248**, 116274.

26 H. Parham and S. Saeed, Pre-concentration and determination of traces of nitrobenzene and 1,3-dinitrobenzene in water samples using anthracite adsorbent, *J. End. Eng. Chem.*, 2014, **20**, 1003.

27 V. M. Gowri and S. A. John, Fabrication of electrically conducting graphitic carbon nitride film on glassy carbon electrode with the aid of amine groups for the determination of an organic pollutant, *J. Electroanal. Chem.*, 2020, **879**, 114787.

28 K. Ahmad and T. H. Oh, Advanced-functional-material-modified electrodes for the monitoring of nitrobenzene: progress in nitrobenzene electrochemical sensing, *Processes*, 2024, **12**, 1884.

29 B. Sharma, S. Jain and N. Dilbaghi, A novel electrochemical sensing platform for detection of nitrobenzene using gadolinium oxide nanorods modified gold electrode, *Indian J. Microbiol.*, 2024, DOI: 10.1007/s12088-024-01372-w.

30 V. Chellappa, N. Meenakshisundaram, J. Annaraj and S. Sagadevan, Hydrothermal synthesis of MnO_2 nanorods for efficient electrochemical detection of environmental anthropogenic pollutants and nitrobenzene, *Inorg. Chem. Commun.*, 2024, **160**, 112015.

31 V. M. Gowri, K. Hemkumar, J. Khumphon, T. Panleam and S. Thongmee, Novel electrochemical platforms for the detection of both clinical disorder biomarker and environmental pollutants using graphitic carbon nitride-conducting oligomer composites, *Microchem. J.*, 2024, **206**, 111555.

32 V. M. Gowri, P. S. Kumar, V. U. Shankar, S. Thongmee and G. Rangasamy, Environmental analysis of nitrobenzene using newly synthesized anisotropic gold nanostructures: Reaction kinetics and electrocatalytic activity, *J. Mol. Liq.*, 2024, **408**, 125303.

33 S. B. Revin and S. A. John, Electropolymerization of 3-amino-5-mercapto-1,2,4-triazole on glassy carbon electrode and its electrocatalytic activity towards uric acid, *Electrochim. Acta*, 2011, **56**, 8934.

34 I. Gallardo, J. Pinson and N. Vila, Spontaneous Attachment of Amines to Carbon and Metallic Surfaces, *J. Phys. Chem. B*, 2006, **110**, 19521.

35 B. Lertanantawong, A. P. O'Mullane, J. Zhang, W. Surareungchai, M. Somasundrum and A. M. Bond, Investigation of mediated oxidation of ascorbic acid by ferrocene methanol using large-amplitude Fourier transformed ac voltammetry under quasi-reversible electron-transfer conditions at an indium tin oxide electrode, *Anal. Chem.*, 2008, **80**, 6515.

36 K. Nakamoto, *Infra-red and Raman Spectra of Inorganic and Coordination Compounds*, Wiley Inter science, 3rd edn, New York, 1978.

37 P. Kalimuthu and S. A. John, Simultaneous determination of epinephrine, uric acid and xanthine in the presence of ascorbic acid using an ultrathin polymer film of 5-amino-1,3,4-thiadiazole-2-thiol modified electrode, *Anal. Chim. Acta*, 2009, **647**, 97.

38 A. Jakhmola, M. Celentano, R. Vecchione, A. Manikas, E. Battista, V. Calcagno and P. A. Netti, Self-assembly of gold nanowire networks into gold foams: production, ultrastructure and applications, *Inorg. Chem. Front.*, 2017, **4**, 1033.

39 P. Kannan and S. A. John, Fabrication of conducting polymer-gold nanoparticles film on electrodes using monolayer protected gold nanoparticles and its electrocatalytic application, *Electrochim. Acta*, 2011, **56**, 7029.

40 V. M. Gowri, A. Ajith, P. S. Kumar, T. Imboon, S. A. John, S. Thongmee and G. Rangasamy, Anisotropic gold nanostructure-mediated electrocatalysis on exfoliated GCN: A shape-dependent study, *Surf. Interface*, 2024, **55**, 105453.

41 N. S. K. Gowthaman, B. Sinduja and S. A. John, Tuning the composition of gold–silver bimetallic nanoparticles for the electrochemical reduction of hydrogen peroxide and nitrobenzene, *RSC Adv.*, 2016, **6**, 63433.

42 F. C. Anson, Innovations in the Study of Adsorbed Reactants by Chronocoulometry, *Anal. Chem.*, 1966, **38**, 54.

43 V. M. Gowri and S. A. John, Fabrication of bulk, nanosheets and quantum dots of graphitic carbon nitride on electrodes:

Morphology dependent electrocatalytic activity, *J. Electroanal. Chem.*, 2021, **895**, 115474.

44 V. M. Gowri, A. Ajith and S. A. John, Systematic Study on Morphological, Electrochemical Impedance, and Electrocatalytic Activity of Graphitic Carbon Nitride Modified on a Glassy Carbon Substrate from Sequential Exfoliation in Water, *Langmuir*, 2021, **37**, 10538.

45 G. Xu, B. Li, X. Wang and X. Luo, Electrochemical sensor for nitrobenzene based on carbon paste electrode modified with a poly(3,4-ethylenedioxythiophene) and carbon nanotube nanocomposite, *Microchim. Acta*, 2014, **181**, 463.

46 J. Ren, L. Li, M. Cui, M. Zhai, C. Yu and X. Ji, Nitrobenzene electrochemical sensor based on silver nanoparticle supported on poly-melamine functional multi-walled carbon nanotubes, *Ionics*, 2016, **22**, 1937.

47 K. Chelladurai, K. Muthupandi, S. M. Chen, M. A. Ali, P. Selvakumar, A. Rajan, P. Prakash, F. M. A. Al-Hemaid and B. S. Lou, Green synthesized silver nanoparticles decorated on reduced graphene oxide for enhanced electrochemical sensing of nitrobenzene in waste water samples, *RSC Adv.*, 2015, **5**, 31139.

48 H. Li, C. Huang, Y. Li, W. Yang and F. Liu, Electrocatalytic reduction of trace nitrobenzene using a graphene-oxide@polymerized manganese porphyrin composite, *RSC Adv.*, 2019, **9**, 22523.

49 C. Pandiyarajan, P. R. Kumar, S. Murugesan and M. Selvara, Silver nanoparticles-supported graphitic-like carbon nitride for the electrochemical sensing of nitrobenzene and its derivatives, *J. Mater. Sci.: Mater. Electron.*, 2021, **32**, 19912.

50 P. Arul and S. A. John, Size controlled synthesis of Ni-MOF using polyvinylpyrrolidone: new electrode material for the trace level determination of nitrobenzene, *J. Electroanal. Chem. B*, 2018, **829**, 168.

51 V. M. Kariuki, S. A. F. Ahmada, F. J. Osongaa and O. A. Sadik, Electrochemical sensor for nitrobenzene using πconjugated polymer-embedded nanosilver, *Analyst*, 2016, **141**, 2259.

52 P. K. Rastogi, V. Ganesan and S. Krishnamoorthi, Palladium nanoparticles incorporated polymer-silica nanocomposite based electrochemical sensing platform for nitrobenzene detection, *Electrochim. Acta*, 2014, **147**, 442.

53 Q. Dong and X. Sun, Enhanced electrochemical detection of nitrobenzene using zinc oxide-carboxylated graphene oxide composite as sensor, *Int. J. Electrochem. Sci.*, 2023, **18**, 100344.